

HOT-JUPITER INFLATION DUE TO DEEP ENERGY DEPOSITION

SIVAN GINZBURG AND RE'EM SARI

Racah Institute of Physics, The Hebrew University, Jerusalem 91904, Israel

Draft version March 1, 2024

ABSTRACT

Some extrasolar giant planets in close orbits—“hot Jupiters”—exhibit larger radii than that of a passively cooling planet. The extreme irradiation L_{eq} these hot Jupiters receive from their close in stars creates a thick isothermal layer in their envelopes, which slows down their convective cooling, allowing them to retain their inflated size for longer. This is yet insufficient to explain the observed sizes of the most inflated planets. Some models invoke an additional power source, deposited deep in the planet’s envelope. Here we present an analytical model for the cooling of such irradiated, and internally heated gas giants. We show that a power source L_{dep} , deposited at an optical depth τ_{dep} , creates an exterior convective region, between optical depths $L_{\text{eq}}/L_{\text{dep}}$ and τ_{dep} , beyond which a thicker isothermal layer exists, which in extreme cases may extend to the center of the planet. This convective layer, which occurs only for $L_{\text{dep}}\tau_{\text{dep}} > L_{\text{eq}}$, further delays the cooling of the planet.

Such a planet is equivalent to a planet irradiated with $L_{\text{eq}}(1 + L_{\text{dep}}\tau_{\text{dep}}/L_{\text{eq}})^\beta$, where $\beta \approx 0.35$ is an effective power-law index describing the radiative energy density as function of the optical depth for a convective planet $U \propto \tau^\beta$. Our simple analytical model reproduces the main trends found in previous numerical works, and provides an intuitive understanding. We derive scaling laws for the cooling rate of the planet, its central temperature, and radius. These scaling laws can be used to estimate the effects of tidal or Ohmic dissipation, wind shocks, or any other mechanism involving energy deposition, on sizes of hot Jupiters.

Subject headings: planetary systems — planets and satellites: general

1. INTRODUCTION

Hot Jupiters are a class of giant planets that orbit their parent stars much closer than Jupiter orbits the sun, therefore exhibiting high surface temperatures (see, e.g. Mayor & Queloz 1995). The observed radii of many of these exoplanets are greater than Jupiter’s radius R_J , with the largest planets reaching radii $\sim 2R_J$ (Baraffe et al. 2010; Anderson et al. 2011; Chan et al. 2011; Hartman et al. 2011; Spiegel & Burrows 2013). This discovery challenges theoretical evolution models, which predict that gas giants cool and contract to smaller radii, closer to $1.0R_J$, at their inferred age, which is often greater than 1Gyr (Burrows et al. 2000, 2007; Laughlin et al. 2005). To some extent, the larger radii are the result of the intense stellar irradiation, which induces a deep radiative, nearly isothermal, layer at the outer edge of the otherwise fully convective planets (Guillot et al. 1996; Arras & Bildsten 2006). This radiative layer slows down the evolutionary cooling of the planet significantly, in comparison with isolated planets (Burrows et al. 2000; Chabrier et al. 2004). The slower cooling results in a higher bulk entropy at a given age, and therefore, a larger radius (see, e.g. Arras & Bildsten 2006; Spiegel & Burrows 2012; Marleau & Cumming 2014).

Yet, the radii of at least some of the inflated hot Jupiters exceed theoretical evolutionary models, even with stellar irradiation taken into account (Baraffe et al. 2003; Burrows et al. 2007; Liu et al. 2008). To settle this discrepancy, a number of explanations have been suggested (see Baraffe et al. 2010; Fortney & Nettelmann 2010; Spiegel & Burrows 2013; Baraffe et al. 2014, for comprehensive reviews).

The different explanations may be divided into several categories. While some works study the effects of extra power, deposited at some depth inside the planet, other focus on enhanced atmospheric opacities (Burrows et al. 2007), suppression of convective heat loss (double-diffusive convection, see Chabrier & Baraffe 2007; Leconte & Chabrier 2012), turbulent mixing (Youdin & Mitchell 2010), or more consistent coupling of the day side and night side of the planet, and taking into account the three-dimensional nature of the problem (Hansen 2008; Guillot 2010; Spiegel & Burrows 2010, 2013; Budaj et al. 2012; Dobbs-Dixon et al. 2012; Perez-Becker & Showman 2013; Mayne et al. 2014; Rauscher & Showman 2014).

In this work we focus on the effects of extra power sources deep in the planet. Possible heat sources include tidal dissipation due to orbital eccentricity (Bodenheimer et al. 2001, 2003; Gu et al. 2003; Winn & Holman 2005; Jackson et al. 2008; Liu et al. 2008; Ibgui & Burrows 2009; Miller et al. 2009; Ibgui et al. 2010, 2011; Leconte et al. 2010), “thermal tides” (Arras & Socrates 2009a,b, 2010; Socrates 2013), Ohmic heating (Batygin & Stevenson 2010; Perna et al. 2010, 2012; Batygin et al. 2011; Huang & Cumming 2012; Rauscher & Menou 2013; Wu & Lithwick 2013; Rogers & Showman 2014), and conversion of a portion of the absorbed stellar flux into kinetic energy in the atmosphere, which is then dissipated at a greater depth (Guillot & Showman 2002; Showman & Guillot 2002). While some of these mechanisms (e.g. Ohmic heating, kinetic energy dissipation) are driven by the stellar irradiation, others (e.g. tidal dissipation) are not. If, as some studies suggest, excess

planet inflation is correlated with the stellar irradiation (Laughlin et al. 2011; Schneider et al. 2011), then the former class of heat deposition mechanisms is favored.

We do not attempt to determine which power sources are more plausible. Alternatively, in the current work we study the effects of a general power source on the cooling, and therefore the radius, of a hot Jupiter. Specifically, we are interested in the dependence of the planet’s cooling history on the amount of additional power, and on the depth at which this power is deposited inside the planet. Recently, Spiegel & Burrows (2013) have conducted such a study numerically (see also Guillot & Showman 2002; Baraffe et al. 2003). In this work we present a simple analytical model for the cooling of insulated gas giants in the presence of heat deposition somewhere in their envelope. Despite our simplifications, this model describes the essential processes, and provides an intuitive explanation to the main trends of the scenario.

The outline of the paper is as follows. In Section 2 we present our model for irradiated planets, without additional heat sources. The effects of additional deposited heat are studied in Sections 3 and 4. In Section 5 we compare our results to the calculations of Spiegel & Burrows (2013), and the main conclusions are summarized in Section 6.

2. IRRADIATED PLANETS

In this section we present our simplified “toy model” for irradiated gas giants, without additional heat sources. The model is one dimensional, and does not differentiate between the day and night sides of the planet (see Spiegel & Burrows 2013). Many aspects of the deposition-free model are essentially similar to a previous analytical work by Arras & Bildsten (2006), and are also implemented by Youdin & Mitchell (2010).

Isolated gas giants, such as Jupiter, are almost fully convective, with convection beginning at an optical depth $\tau \sim 1$ (Trafton 1964, 1967; Hubbard 1968; Stevenson & Salpeter 1977); see also Guillot et al. (1994) for a reexamination. Insolated planets, on the other hand, are expected to develop a deep radiative envelope (Guillot et al. 1996).

2.1. Convective Interior Structure

The analysis of irradiated planets is simpler when considering their profiles in the (τ, U) plane, with

$$\tau(r) = \int_r^R \kappa \rho dr' \quad (1)$$

denoting the optical depth at radius r , from the planet surface, at radius R , and $U \equiv aT^4$ is the radiative energy density. The density, temperature, and opacity are denoted by ρ , T , and κ , respectively, and a is the radiation constant. Our main simplification is to assume that this profile can be approximated by a power law in the convective interior

$$\frac{U}{U_c} = \left(\frac{\tau}{\tau_c} \right)^\beta, \quad (2)$$

with $U_c \equiv aT_c^4$ denoting the central radiation energy density, determined by the central temperature T_c .

This scaling can be derived in the case of a power-law opacity $\kappa \propto \rho^a T^b$, as assumed by Arras & Bildsten

(2006) and Youdin & Mitchell (2010). The opacity is combined with the adiabatic temperature and pressure relation in the convective region (see, e.g., Hubbard 1977; Saumon et al. 1996) $T \propto P^{1/(n+1)}$, and the resulting polytropic density profile at the edge of the planet $\rho \approx \rho_c(1 - r/R)^n$ (ρ_c denotes the central density; see, e.g., Matzner & McKee 1999). We neglect super-adiabatic corrections to the convective temperature profile (Trafton 1967; Chabrier & Baraffe 2007). These power laws yield

$$\beta = \frac{4}{b + 1 + n(a + 1)}, \quad (3)$$

and $\tau_c \sim \kappa_c \rho_c R$, with κ_c denoting the estimate for the central opacity, if the power-law opacity could be continued to the center.

The Rosseland opacity (we assume a gray approximation) in the range of interest is depicted in Figure 1 of Arras & Bildsten (2006). The molecular dominated opacity below $T_0 \approx 2500\text{K}$ is fit by $a = b = 0.5$. Above T_0 , the opacity rises steeply, with $b = 7$ ($a = 0.5$), due to H^- , whose population increases primarily as a consequence of metal ionization (see, e.g., Kippenhahn & Weigert 1994). At even higher temperatures, above $\sim 10^4\text{K}$, the H^- vanishes, due to lack of neutral hydrogen, and the opacity is given by the Kramers bound-free opacity law, with $a = 1$, $b = -3.5$ (see, e.g., Kippenhahn & Weigert 1994; Padmanabhan 2000).

As explained in Sections 2.3 and 2.4, the internal luminosity of a planet is determined by the location of the radiative-convective boundary. The optical depth (and pressure level) of this boundary is given by the opacity power-law which is suitable for the (almost isothermal) radiative-zone temperature, and does not depend on the deeper opacity structure. For planets without additional heating, this temperature is typically below T_0 , and we therefore get $\beta = 0.8$, by taking $n \approx 2$ (Peebles 1964; Hubbard 1977; Saumon et al. 1996). Throughout the majority of this work we adopt the approximation of small inflations relative to the zero-temperature radius (see Section 4), implying roughly constant central densities and pressures. Consequently, a constant $\tau_c = \tau_0 \sim 10^{11}$ is suitable for a Jupiter-size planet. Inspection of numerical evolution models (see Table 1 in Burrows et al. 1997) reveals that the ratio between central and photosphere temperatures, which is given by setting $\tau \sim 1$ in Equation (2), $T_c/T_{\text{ph}} = \tau_c^{\beta/4}$, is ~ 100 , and changes only by a factor of 2 during the cooling of a Jupiter mass isolated planet, consistent with our estimate.

In Section 3 we show that heat deposition raises the radiative-convective boundary temperature above T_0 , requiring a more general form, which takes into account the strong dependence of the H^- opacity on the temperature

$$\frac{\tau_c}{\tau_0} = \left(\frac{T_c}{T_0} \right)^b. \quad (4)$$

In this case we get $\beta = 0.35$ from Equation (3), which is suitable for temperatures above T_0 . As we show in Section 2.3, the convective profile must satisfy $\beta < 1$.

2.2. Radiative Envelope Structure

Proximity to a star dictates an equilibrium temperature T_{eq} on the planet surface, which we take as the photosphere, at $\tau \sim 1$. Our model is spherical so we assume an even distribution of the absorbed heat over the planet surface, for which (see, e.g., Guillot et al. 1996)

$$T_{\text{eq}} = (1 - A)^{1/4} T_{\odot} \left(\frac{R_{\odot}}{2D} \right)^{1/2}, \quad (5)$$

with T_{\odot} and R_{\odot} denoting the stellar temperature and radius, respectively, and D , A are the planet's orbital distance and albedo, respectively. This equilibrium temperature defines an energy density $U_{\text{eq}} \equiv aT_{\text{eq}}^4$, and luminosity $L_{\text{eq}} \equiv 4\pi R^2 \sigma T_{\text{eq}}^4$, where σ is the Stefan-Boltzmann constant.

The radiation energy is related to the internal luminosity of the planet L_{int} through the diffusion approximation

$$\frac{L_{\text{int}}}{4\pi R^2} = \frac{c}{3} \frac{dU}{d\tau}, \quad (6)$$

where c is the speed of light. Close to the surface, L_{int} is constant (in space), since it is the result of cooling of the entire planet, and the heat capacity of the outer layers is negligible. Therefore, we can integrate Equation (6) and find the radiative profile

$$U = U_{\text{eq}} + \frac{3}{c} \frac{L_{\text{int}}}{4\pi R^2} \tau, \quad (7)$$

where the distinction between the boundary conditions $U = U_{\text{eq}}$ at $\tau = 0$ and $\tau \sim 1$ is negligible, since we are generally interested in $\tau \gg 1$. Bodenheimer et al. (2003) use a similar boundary condition (with $U = U_{\text{eq}}$ at $\tau = 2/3$), while Arras & Bildsten (2006) and Youdin & Mitchell (2010) define a temperature T_{deep} for their boundary condition, which is correlated with T_{eq} , therefore leading to similar conclusions. More elaborate boundary conditions, which incorporate a frequency-dependent opacity, and require the solution of the radiative transfer equation, or the use of a two-stream approximation (Barman et al. 2001; Hubeny et al. 2003; Hansen 2008; Guillot 2010; Guillot & Havel 2011), are beyond the scope of this work, and their effect on the temperature deep inside the radiative zone (and therefore on the cooling rate) can be modeled by a somewhat different effective T_{eq} . We remark that an atmosphere which is more transparent in the optical regime (although this does not seem to be the case for hot Jupiters; see, e.g., Spiegel & Burrows 2013) may induce a greenhouse effect, which can be treated with our model as heat deposited at $\tau > 1$, where the depth for optical light is unity.

Planar symmetry, and the focus on the outer layers of the planet throughout this work, are justified both self-consistently in Section 2.4, and by Guillot et al. (1996), who find that during the 10 Gyr evolution of a hot Jupiter, the radiative region penetrates only a few percent of the radius.

2.3. Radiative-Convective Transition

According to the Schwarzschild criterion, when the radiative temperature gradient becomes larger than the adiabatic gradient, convective instability develops. Differentiating Equations (2) and (7) shows that convection

sets in when

$$\frac{4}{3} \frac{L_{\text{eq}}}{L_{\text{int}}} \frac{1}{\tau} < \frac{1 - \beta}{\beta}. \quad (8)$$

We see from Equation (8) that at $\tau \rightarrow 0$ the profile is radiative. We also see that to ensure convection at $\tau \rightarrow \infty$, we must have $\beta < 1$.

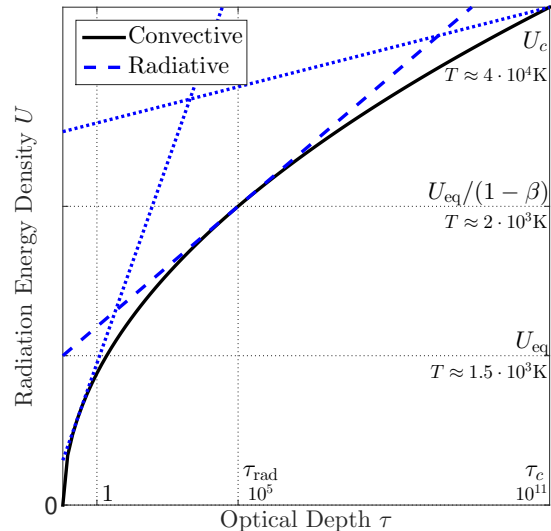


FIG. 1.— Transition between convective (solid black line) and radiative (dashed blue line) profiles. The convective profile follows Equation (2), while the radiative profile is according to Equation (7). The combined profile follows the radiative profile for $\tau < \tau_{\text{rad}}$, and the convective profile for $\tau > \tau_{\text{rad}}$. Two additional extreme cases are plotted for the same values of U_c and τ_c (dotted blue lines). A very high value $U_{\text{eq}} > U_c(1 - \beta)$ corresponds to a fully radiative planet, while a very low value of U_{eq} leads to $\tau_{\text{rad}} < 1$, and therefore a fully convective planet. Typical values of the optical depth and temperature are given.

The transition between convective and radiative profiles is illustrated schematically in Figure 1. For a planet with given interior (U_c , τ_c) and exterior (U_{eq}) boundary conditions, the convective profile is given by Equation (2), while the radiative profile is given by Equation (7). Since the radiative profile is linear in τ , the luminosity L_{int} and the radiative-convective transition point τ_{rad} are calculated by finding the tangent to the adiabatic profile. For $\tau < \tau_{\text{rad}}$, the radiative gradient is smaller than the adiabatic, so the profile is radiative. For $\tau > \tau_{\text{rad}}$, the radiative gradient is larger than the adiabatic, so the profile is convective. Quantitatively, the tangency point is found by equating Equations (2) and (7) and their derivatives. The solution for τ_{rad} is

$$\left(\frac{\tau_{\text{rad}}}{\tau_c} \right)^\beta = \frac{1}{1 - \beta} \frac{U_{\text{eq}}}{U_c}, \quad (9)$$

which corresponds to a radiation energy density

$$U(\tau_{\text{rad}}) = \frac{1}{1 - \beta} U_{\text{eq}}, \quad (10)$$

implying that the radiative zone is isothermal to within a factor of $(1 - \beta)^{-1/4} \approx 1.5$. Equation (9) indicates that the radiative region thickens with increasing solar irradiation and with decreasing central tempera-

ture (see also Guillot et al. 1996; Burrows et al. 2000; Arras & Bildsten 2006; Youdin & Mitchell 2010).

2.4. Internal Luminosity and Cooling

Equations (8) and (9) connect the internal luminosity to the central temperature

$$\frac{L_{\text{int}}}{L_{\text{eq}}} \sim \frac{1}{\tau_{\text{rad}}} \sim \frac{1}{\tau_c} \left(\frac{U_c}{U_{\text{eq}}} \right)^{1/\beta}. \quad (11)$$

Note that Equation (11) breaks down when $\tau_{\text{rad}} \lesssim 1$. In this case, the planet is considered to be fully convective, and its luminosity is determined by the radiation energy density at the photosphere U_{ph} . Substituting $\tau = 1$ in Equation (2) we find

$$U_{\text{ph}} = U_c \left(\frac{1}{\tau_c} \right)^\beta, \quad (12)$$

and luminosity

$$\frac{L_{\text{int}}}{L_{\text{eq}}} = \frac{U_{\text{ph}}}{U_{\text{eq}}} = \left(\frac{1}{\tau_c} \right)^\beta \frac{U_c}{U_{\text{eq}}}. \quad (13)$$

Comparing Equations (9) and (12) shows that the condition $\tau_{\text{rad}} \lesssim 1$ is equivalent to the condition $U_{\text{ph}} \gtrsim U_{\text{eq}}$. In other words, as long as the central temperature of the planet is high enough to ensure that a convective profile will reach $\tau \sim 1$ without dropping below T_{eq} , the planet remains fully convective. However, as the planet cools, the central temperature decreases, and the convective profile would have predicted temperatures below T_{eq} . This situation is unphysical, and an approximately isothermal radiative zone develops.

To summarize, using Equations (11) and (13), the internal luminosity of the planet, as a function of its central radiation energy density is given by

$$\frac{L_{\text{int}}}{L_{\text{eq}}} \sim \begin{cases} \frac{1}{\tau_c} \left(\frac{U_c}{U_{\text{eq}}} \right)^{1/\beta} & \frac{U_c}{U_{\text{eq}}} < \tau_c^\beta \\ \left(\frac{1}{\tau_c} \right)^\beta \frac{U_c}{U_{\text{eq}}} & \frac{U_c}{U_{\text{eq}}} > \tau_c^\beta \end{cases}, \quad (14)$$

where the transition is when $\tau_{\text{rad}} \sim L_{\text{eq}}/L_{\text{int}} \sim 1$. Since $\beta < 1$, Equation (14) indicates that the proximity to a star, which is manifested for $U_c/U_{\text{eq}} < \tau_c^\beta$, diminishes the internal luminosity and slows down the planet's cooling (see also Guillot et al. 1996; Burrows et al. 2000; Arras & Bildsten 2006; Youdin & Mitchell 2010; Spiegel & Burrows 2013).

As a planet cools, it makes the transition from an isolated planet, which is not affected by stellar irradiation, and matches the high U_c limit of Equation (14), to an insulated planet, which matches the low U_c limit. The age, at which this transition takes place, may be estimated by writing an evolution equation for the central temperature of an isolated planet

$$L_{\text{int}} \sim -k_B \frac{M}{m_p} \frac{dT_c}{dt}, \quad (15)$$

where k_B is Boltzmann's constant, m_p is the proton mass, M is the mass of the planet, and t denotes time. Equation (15) is valid for the cooling degenerate phase of the planet's evolution, which follows

a rapid non-degenerate contraction phase (see Guillot 2005; Arras & Bildsten 2006). Substituting the luminosity from Equation (14), we get

$$\frac{4\pi R^2 \sigma T_c^4}{\tau_c^\beta} \sim -k_B \frac{M}{m_p} \frac{dT_c}{dt}. \quad (16)$$

Assuming that the planet cools down from high temperatures, Equation (16) predicts the cooling time to a temperature $T_c = T_{\text{eq}} \tau_c^{\beta/4}$, which marks the transition to the insulated regime (at this stage the photosphere reaches a temperature $T_{\text{ph}} \sim T_{\text{eq}}$):

$$t \sim \frac{M}{m_p} \frac{k_B}{12\pi R^2 \sigma T_{\text{eq}}^3} \tau_c^{\beta/4} \approx 7 \text{ Myr} \left(\frac{10^3 \text{ K}}{T_{\text{eq}}} \right)^3, \quad (17)$$

where the numerical value is estimated for M_J (Jupiter mass) and R_J . This estimate roughly fits Jupiter, which is a few Gyr old (Guillot 2005), has an equilibrium temperature $T_{\text{eq}} \approx 110 \text{ K}$, and is close to the transition, since $T_{\text{ph}} \approx 120 \text{ K}$ (Hanel et al. 1981). Strongly irradiated planets orbit their parent star closer than Jupiter by a factor of 100, thus having, using Equation (5), $T_{\text{eq}} \sim 10^3 \text{ K}$, and therefore reach the insulated regime and develop a radiative zone after less than 10^7 years (consistent with Guillot et al. 1996).

In the following, insulated stage of planetary evolution, Equation (15) is combined with the low U_c limit of Equation (14) to produce a cooling equation

$$T_c(t) \sim \left[\tau_c k_B \frac{M}{m_p} \frac{T_{\text{eq}}^{4(1-\beta)/\beta}}{4\pi R^2 \sigma} \frac{1}{t} \right]^{\beta/(4-\beta)} \quad (18)$$

$$\approx 6 \cdot 10^4 \text{ K} \left(\frac{T_{\text{eq}}}{10^3 \text{ K}} \right)^{1/4} \left(\frac{1 \text{ Gyr}}{t} \right)^{1/4},$$

with the numerical values estimated for M_J , R_J . This result is consistent with Guillot et al. (1996). At an age of 8 Gyr, the radiative region encompasses a few percent in radius, $1 - r/R \sim (\rho/\rho_c)^{1/n} \sim T_{\text{eq}}/T_c$, consistent with Guillot et al. (1996), and self-consistently justifying our focus on the outer layers of the planet.

A third stage in a cooling planet's life, equilibrium, is reached when $U_c = U_{\text{eq}}$. In this case, according to Equation (9), the planet becomes fully radiative, and the luminosity vanishes $L_{\text{int}} = 0$ (since the temperature gradient vanishes). This condition determines the planet's equilibrium central temperature, and therefore its equilibrium radius. More precisely, the planet becomes fully radiative when U_c drops below $U_{\text{eq}}/(1 - \beta)$. It is easy to see, from Equation (18), that without additional heat deposition, planets never reach equilibrium (the timescales are too long).

The three stages of planetary evolution, described in this section, are displayed in Figure 1, for planets with the same central temperature and optical depth, but different equilibrium temperatures.

3. DEPOSITION OF ADDITIONAL POWER

In this section we discuss how the internal luminosity is affected by an additional heat source, which deposits power at some depth inside the planet. Our goal is to find $L_{\text{int}}(T_{\text{eq}}, T_c, L_{\text{dep}}, \tau_{\text{dep}})$, with L_{dep} denoting the deposited luminosity, and τ_{dep} denoting the optical depth

where the power is deposited. In Section 2.4, and specifically in Equation (14), we found $L_{\text{int}}(L_{\text{dep}} = 0)$, which we abbreviate hereafter as L_{int}^0 . We focus on planets which have developed a substantial radiative zone, $\tau_{\text{rad}} > 1$, so L_{int}^0 is determined by the low U_c limit of Equation (14). The motivation is that strongly irradiated planets develop such a radiative zone in less than 10^7 years, as explained in Section 2.4 (see also Guillot et al. 1996).

Without heat sources, the radiative zone is described by Equation (7). The addition of a deposited power L_{dep} at τ_{dep} introduces a jump in the profile slope. Explicitly, the radiative profile is altered:

$$\frac{dU}{d\tau} = \frac{3}{4\pi R^2 c} \cdot \begin{cases} L_{\text{tot}} \equiv L_{\text{int}} + L_{\text{dep}} & \tau < \tau_{\text{dep}} \\ L_{\text{int}} & \tau > \tau_{\text{dep}} \end{cases}, \quad (19)$$

with L_{tot} denoting the total luminosity for $\tau < \tau_{\text{dep}}$. The radiative profile, with deposited heat included, is displayed in Figure 2. As seen in Figure 2, the deposited heat effectively changes U_{eq} to some higher $U_{\text{eq}}^{\text{eff}}$. The internal luminosity L_{int} is found, as in Section 2.3, by calculating the tangent from the point $[\tau_{\text{dep}}, U(\tau_{\text{dep}})]$ to the convective profile, which is equivalent to calculating the tangent from the point $[0, U_{\text{eq}}^{\text{eff}}]$. Therefore, the results of Section 2.3 are reproduced, but with $U_{\text{eq}}^{\text{eff}}$ instead of U_{eq} . Since, from Equation (11), $L_{\text{int}} \propto U_{\text{eq}}^{-(1-\beta)/\beta}$, the internal luminosity decreases. This result is also evident graphically in Figure 2: the slope of the radiative tangent decreases, as well as the deeper penetration of the radiative zone into the planet interior.

3.1. Secondary Convective Region

In Figure 2 we assumed that the outer layers remain radiative. However, if the total power, L_{tot} , which has to be evicted from the planet, is high enough, then it cannot be delivered radiatively, and a secondary convective instability develops. According to Equations (8) and (19), with L_{tot} replacing L_{int} as the evicted power, convection appears at an optical depth

$$\tau_b = \frac{4}{3} \frac{\beta}{1-\beta} \frac{L_{\text{eq}}}{L_{\text{tot}}}, \quad (20)$$

where the radiation energy density reaches $U_{\text{eq}}/(1-\beta)$. If we focus on intense deposition $L_{\text{dep}} \gg L_{\text{int}}$, then we may approximate $L_{\text{tot}} \approx L_{\text{dep}}$, and using Equation (20), $\tau_b \sim L_{\text{eq}}/L_{\text{dep}}$.

The temperature profile, with deposited heat added, can be divided into two cases, depending on L_{dep} and τ_{dep} . If $\tau_{\text{dep}} < \tau_b$, or equivalently $L_{\text{dep}}\tau_{\text{dep}}/L_{\text{eq}} \lesssim 1$, the depiction in Figure 2 is accurate. As seen in Figure 2, in this case $U_{\text{eq}}^{\text{eff}}$ is restricted by a maximal value $U_{\text{eq}}^{\text{eff}} < U_{\text{eq}}/(1-\beta)$, limiting the reduction in internal luminosity, using Equation (11), to an insignificant effect $L_{\text{int}}/L_{\text{int}}^0 > (1-\beta)^{(1-\beta)/\beta} \sim 1$.

In the case where $\tau_{\text{dep}} > \tau_b$, a secondary convective region emerges between τ_b and τ_{dep} . This region is displayed in Figure 3. The modified luminosity can be calculated by finding $U_{\text{eq}}^{\text{eff}}$. Using Equation (20), approximating $L_{\text{dep}} \gg L_{\text{int}}$, and noting that in this regime

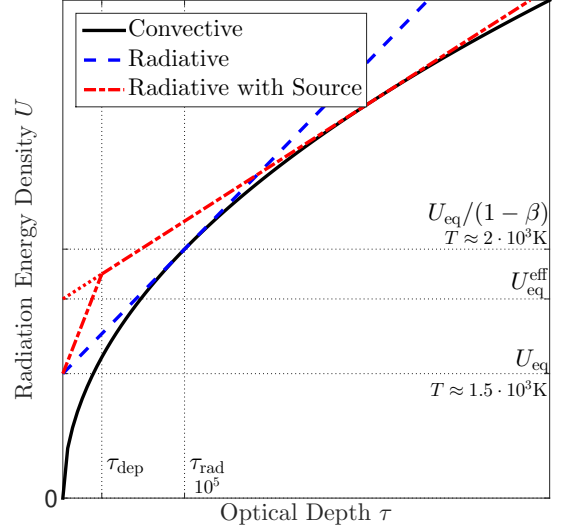


FIG. 2.— Modification of the radiative profile due to the deposition of heat at optical depth τ_{dep} . The convective profile (solid black line), and the radiative profile without a heat source (dashed blue line) are similar to Figure 1. The modified radiative profile (dot-dashed red line) is described by Equation (19). The imaginary continuation of the profile with a slope $3L_{\text{int}}/(4\pi R^2 c)$ down to $\tau = 0$ (dotted red line) defines $U_{\text{eq}}^{\text{eff}}$. As in Figure 1, the combined profile follows the radiative profile up to the tangency point, and then it follows the convective profile.

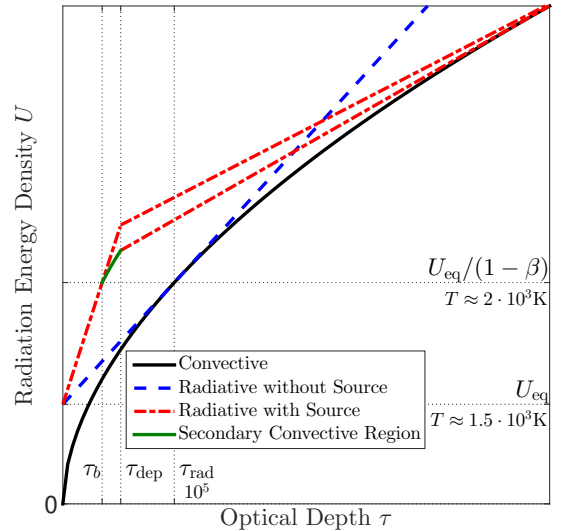


FIG. 3.— Emergence of a secondary convective region from τ_b to τ_{dep} (solid green line). The convective (solid black line) and radiative (dashed blue line) profiles without a heat source are similar to Figures 1 and 2. The radiative profile with heat deposited at τ_{dep} (upper dot-dashed red line) is similar to Figure 2, and is inadequate in this case. Due to the secondary convective region, the radiative profile is altered, and it follows the lower dot-dashed red line, up to the tangency point with the main convective profile.

$L_{\text{dep}}\tau_{\text{dep}}/L_{\text{eq}} \gtrsim 1$, we find

$$\frac{U_{\text{eq}}^{\text{eff}}}{U_{\text{eq}}} \approx \frac{1}{1-\beta} \frac{U(\tau_{\text{dep}})}{U(\tau_b)} \sim \left(\frac{L_{\text{dep}}\tau_{\text{dep}}}{L_{\text{eq}}} \right)^\beta, \quad (21)$$

where $U(\tau_{\text{dep}})$ is adiabatically related to $U(\tau_b)$. Combining this result with Equation (11), we get $L_{\text{int}}/L_{\text{int}}^0 \sim$

$(L_{\text{dep}}\tau_{\text{dep}}/L_{\text{eq}})^{-(1-\beta)}$, which we rewrite as

$$\frac{L_{\text{int}}}{L_{\text{int}}^0} \sim \left(1 + \frac{L_{\text{dep}}\tau_{\text{dep}}}{L_{\text{eq}}}\right)^{-(1-\beta)}, \quad (22)$$

in order to interpolate with the $L_{\text{dep}}\tau_{\text{dep}}/L_{\text{eq}} \lesssim 1$ regime.

Equation (22) shows that the figure of merit of the heat source, in terms of its influence on the internal luminosity, is $L_{\text{dep}}\tau_{\text{dep}}/L_{\text{eq}}$, which must satisfy $L_{\text{dep}}\tau_{\text{dep}}/L_{\text{eq}} \gtrsim 1$ for a significant effect. For example, if the heat is deposited at $\tau_{\text{dep}} \sim 1$, then $L_{\text{dep}} \gtrsim L_{\text{eq}}$ is needed. This result is intuitive, since the equilibrium luminosity itself is deposited at $\tau \sim 1$. If, on the other hand, the heat is deposited at the top of the convective region, $\tau_{\text{dep}} \sim \tau_{\text{rad}}$, then, using Equation (11), $L_{\text{dep}} \gtrsim L_{\text{int}}^0$ is sufficient. Although not evident from Equation (22), $L_{\text{dep}} > L_{\text{int}}^0$ is required for a significant effect (see also Guillot & Showman 2002), even for deposition in the convective region $\tau_{\text{dep}} > \tau_{\text{rad}}$. Otherwise, the deposited power simply replaces part of the internal luminosity as the convectively delivered heat which maintains the radiative profile at the envelope, and the temperature profile remains unchanged (with respect to $L_{\text{dep}} = 0$). In this case, the luminosity decreases by L_{dep} .

The secondary convective region, described in this section, was also noted in numerical works (Guillot & Showman 2002; Batygin et al. 2011; Wu & Lithwick 2013), for high dissipated power.

3.2. Cooling and Equilibrium

Substantial additional heating raises the effective equilibrium temperature, and therefore the inner radiative-convective boundary temperature above T_0 , as seen in Equation (21). Under the influence of such a heat source, using Equation (22), the cooling Equation (18) in the isolated regime changes to

$$\begin{aligned} T_c(t) &\propto \left(1 + \frac{L_{\text{dep}}\tau_{\text{dep}}}{L_{\text{eq}}}\right)^{\beta(1-\beta)/(4-\beta-\beta b)} \\ &= \left(1 + \frac{L_{\text{dep}}\tau_{\text{dep}}}{L_{\text{eq}}}\right)^{0.19}, \end{aligned} \quad (23)$$

slowing down the planet's cooling, with the power calculated using the H^- opacity values $\beta = 0.35$ and $b = 7$, following the discussion in Section 2.

Equilibrium is reached when $U_c \approx U_{\text{eq}}^{\text{eff}}$ (see Section 2). According to Equations (9) and (21), the required heating intensity for this scenario is

$$\frac{L_{\text{dep}}\tau_{\text{dep}}}{L_{\text{eq}}} \sim \left(\frac{U_c}{U_{\text{eq}}}\right)^{1/\beta} \sim \frac{\tau_c}{\tau_{\text{rad}}}, \quad (24)$$

with τ_{rad} denoting, as before, the original radiative-convective transition, without additional heating. We may rewrite Equation (24), using Equation (11), as $L_{\text{dep}}\tau_{\text{dep}} \sim L_{\text{int}}^0\tau_c$, showing that, as intuitively expected, a deposition of order L_{int}^0 forces equilibrium, when the deposition is at the center. For a given heat source, Equation (24) defines the equilibrium central temperature $T_c = T_{\text{eq}}^{\text{eff}} \equiv (U_{\text{eq}}^{\text{eff}}/a)^{1/4}$, for which evolutionary cooling not only slows down, but stops entirely

$$\frac{T_c}{T_{\text{eq}}} = \frac{T_{\text{eq}}^{\text{eff}}}{T_{\text{eq}}} \sim \left(1 + \frac{L_{\text{dep}}\tau_{\text{dep}}}{L_{\text{eq}}}\right)^{\beta/4}, \quad (25)$$

where we have again interpolated with the weak heating regime.

If, due to very intensive (or deep) heating, $T_{\text{eq}}^{\text{eff}} \gtrsim 10^4\text{K}$, the opacity behaves according to the Kramers law, with $b = -3.5$ and $\beta > 1$, prohibiting convection (see Section 2). In this case, the planet becomes fully radiative from τ_{dep} inward, even before equilibrium is reached. The internal luminosity in this case is given by Equation (6), $L_{\text{int}} \approx (4\pi R^2 c/3)(U_c/\tau_c)$. Combining this result with Equation (15), we find that the cooling time is $t \propto T_c^{-(3-b)} = T_c^{-6.5}$, with hotter (more inflated) planets reaching equilibrium first (planets with radii close to $2R_J$ cool even faster, due to the dependence of the opacity on the density). This regime corresponds to the equilibrium-inflation paradigm of hot Jupiters, which typically involves very deep heating (Guillot & Showman 2002; Chabrier et al. 2004; Burrows et al. 2007; Liu et al. 2008; Spiegel & Burrows 2013).

4. EFFECT OF HEATING ON PLANET RADIUS

In Sections 2 and 3 we found the effects of stellar irradiation and additional heat deposition on the planet luminosity. The diminished luminosity results in slower cooling, and therefore a higher bulk temperature and larger radius at a specific age, in addition to a larger equilibrium radius. For a rough estimate of this inflation, we introduce a simple model which relates the planet's radius R to its central temperature T_c .

We start by writing a simple equation of state (EOS)

$$P = K\rho^{5/3} \left[1 - \left(\frac{\rho_0}{\rho}\right)^{1/3}\right] + \frac{\rho}{m_p}k_B T, \quad (26)$$

where $K \sim h^2/(m_e m_p^{5/3})$ is the electron degeneracy term, and $(\rho_0/m_p)^{1/3} \sim m_e e^2/h^2 \sim a_0^{-1}$ is the electrostatic correction (h denotes the Planck constant, m_e and e denote the electron mass and charge, respectively, and a_0 is the Bohr radius; see, e.g., Padmanabhan 2001, where we assume a mixture of hydrogen and helium, so the atomic weight and charge are approximately 1). The rightmost term is the ideal gas pressure of the non-degenerate ions. We are interested in the regime where the degeneracy parameter $\theta \equiv (\rho k_B T/m_p)/K\rho^{5/3} \sim 10^{-1}$, which is adequate for HD 209458b (see Guillot 2005). In this regime, the electrons are almost completely degenerate, and the ion thermal term is a small correction. Since the degeneracy pressure is inversely related to the particle mass, the ions are non-degenerate. The thermal contribution of the degenerate electrons is quadratic in θ (see, e.g., Chandrasekhar 1939), and is therefore negligible. This EOS is also used by Arras & Bildsten (2006).

We proceed by replacing the profiles $\rho(r), T(r), P(r)$, with the characteristic values ρ_c, T_c, P_c . This simplification is justified by noting that the entire planet (except for the radiative isothermal envelope) can be described approximately with a single almost degenerate polytrope. The distinction between a degenerate core and a non-degenerate envelope is insignificant, since the temperature profile is almost parallel to lines of constant θ (Guillot 2005). A similar argument renders the distinction between a core without electrostatic corrections, and

an envelope with significant corrections, also insignificant in comparison with the bulk electrostatic correction. For a given central temperature T_c , the contribution of the isothermal ($T \approx T_{\text{eq}}$) radiative envelope to the radius is negligible, because it scales with the temperature, and $T_{\text{eq}} \ll T_c$. We emphasize that the quasi-degenerate treatment in this section only holds for mild inflations, and should be taken only as an order of magnitude estimate for extremely inflated planets, with radii $\sim 2R_J$. In these cases, numerical radius-temperature relations are more adequate, as detailed below.

In equilibrium, the pressure of Equation (26) balances the gravitational pressure, of order GM^2/R^4 (G is the gravitational constant),

$$K\rho_c^{5/3} \left[1 - \left(\frac{\rho_0}{\rho_c} \right)^{1/3} \right] + \frac{\rho_c}{m_p} k_B T_c \sim GM^2/R^4 \rho_c^{4/3}. \quad (27)$$

For small variations of the temperature, differentiating Equation (27), while holding the planet mass constant, yields a linear relation

$$\frac{dR}{R} \Big|_M = -\frac{1}{3} \frac{d\rho_c}{\rho_c} \Big|_M = \frac{\frac{\rho_c}{m_p} k_B dT_c}{K\rho_c^{5/3} - \frac{\rho_c}{m_p} k_B T_c}. \quad (28)$$

In the degenerate limit ($\rho_c k_B T_c / m_p \ll K\rho_c^{5/3}$), the radius increases with temperature, while in the non-degenerate limit ($\rho_c k_B T_c / m_p \gg K\rho_c^{5/3}$), the planet shrinks as the temperature increases. As mentioned above, the non-degenerate limit corresponds to the initial contraction phase, accompanied by an increase in temperature, while the degenerate limit describes the later cooling of the planet, which is accompanied by a decrease in radius. The inflated hot Jupiters are on the late-time cooling branch of this scenario (the transition is at a radius around $4R_J$, see Guillot et al. 1996).

We make a linear approximation for low temperatures, using Equations (27) and (28)

$$\begin{aligned} \Delta R &\approx \frac{R^2}{GMm_p} k_B T_c \left[1 + (M_J/M)^{2/3} \right]^{-1} \sim \frac{k_B T_c}{m_p g} \\ &\approx 0.1 R_J \left(\frac{T_c}{10^4 \text{K}} \right), \end{aligned} \quad (29)$$

with $\Delta R \equiv R - R_0$ denoting the inflation relative to the zero-temperature radius R_0 , g is the surface gravity, and noting that Jupiter's mass is close the well-known inversion of the zero-temperature mass-radius relation $M_J \sim (K/G)^{3/2} \rho_0^{1/2}$ (Padmanabhan 2001). Since we focus on hot Jupiters with $M \approx M_J$, the electrostatic correction term M_J/M does not influence our order of magnitude estimate. This relation fits well numerical radius-temperature curves (for example, Burrows et al. 1997, Table 1), up to a radius of $\sim 1.3R_J$, where the linear approximation breaks down (since it assumes $\Delta R \ll R_0 \approx R_J$). See Arras & Bildsten (2006) for a similar linear relation between the radius change and the central temperature.

Although Equation (29) was derived for a constant planet mass, it is also valid (up to numerical factors) when the planet surface gravity g , instead of the planet mass is kept constant. In this case, the gravitational

pressure in Equation (27) may be written as g^2/G , and the radius increase is found by differentiating $dR/R|_g = -d\rho_c/\rho_c|_g$. This scenario is interesting for comparison with the results of Spiegel & Burrows (2013), who studied models with constant surface gravity.

5. COMPARISON TO NUMERICAL CALCULATIONS

Guillot & Showman (2002) and Baraffe et al. (2003) find that less heat dissipation is needed to inflate hot Jupiters if the heat is deposited in deeper mass fractions of the planet (see also Wu & Lithwick 2013). In this section we compare our estimates to the systematic work of Spiegel & Burrows (2013), henceforth SB2013, who studied the effects of different amounts of additional heat, deposited at different pressure levels.

In their Section 3.3, specifically Figure 4, SB2013 deposit different fractions of the incident flux $F_{\text{dep}}/F_{\text{eq}} = L_{\text{dep}}/L_{\text{eq}}$ at different pressures inside a planet similar to HD 209458b. For each value of additional power and deposition pressure, SB2013 present the inflated planet radius. We emphasize that, in their Section 3.3, SB2013 concentrate on planets which have not yet reached equilibrium, but are still contracting. Moreover, they compare models with the same effective temperature, defined as $T_{\text{eff}} \equiv (L_{\text{int}}/\sigma 4\pi R^2)^{1/4}$, and the same surface gravity, resulting in models with different ages and masses.

By combining Equations (14) and (22), we relate the central temperature to the deposited power,

$$\frac{T_c}{T_{\text{eq}}} \sim \left[\tau_0 \left(\frac{T_{\text{eq}}}{T_0} \right)^b \frac{L_{\text{int}}}{L_{\text{eq}}} \left(1 + \frac{L_{\text{dep}} \tau_{\text{dep}}}{L_{\text{eq}}} \right)^{1-\beta} \right]^{\beta/(4-\beta b)}. \quad (30)$$

The inflated planet radius can be related to the deposited power by combining Equation (30) with Equation (29)

$$\begin{aligned} \Delta R &= \frac{k_B T_{\text{eq}}}{m_p g} \left[\tau_0 \left(\frac{T_{\text{eff}}}{T_{\text{eq}}} \right)^4 \left(\frac{T_{\text{eq}}}{T_0} \right)^b \right]^{\beta/(4-\beta b)} \\ &\times \left(1 + \frac{L_{\text{dep}} \tau_{\text{dep}}}{L_{\text{eq}}} \right)^{\beta(1-\beta)/(4-\beta b)} \\ &\equiv \Delta R_0 \left(1 + \frac{L_{\text{dep}} \tau_{\text{dep}}}{L_{\text{eq}}} \right)^{\beta(1-\beta)/(4-\beta b)}, \end{aligned} \quad (31)$$

with $\Delta R_0 = 0.27R_J$ denoting the expansion without extra heating. This numeric value is estimated by substituting the parameters $g = 10^3 \text{ cm s}^{-2}$ and $T_{\text{eff}} = 180\text{K}$, which are kept constant in SB2013, the observed temperature $T_{\text{eq}} = 1300\text{K} \gg T_{\text{eff}}$ (Crossfield et al. 2012), and taking the adequate $\beta = 0.35$ and $b = 7$. The model of SB2013 for HD209458b is indeed inflated by $\Delta R_0 = 1.25R_J - 0.95R_J = 0.30R_J$, due to the irradiation of the parent star, even without extra power sources (see also Baraffe et al. 2003; Burrows et al. 2007), in agreement with our estimate. The zero-temperature radius $R_0 = 0.95R_J$ is estimated using Guillot (2005) and Baraffe et al. (2010), for the given surface gravity. An alternative estimate of the inflation may be given by relating the central temperature, found in Equation (30), to ΔR , using the numerically calculated $R(T_c)$ curve given in Burrows et al. (1997). This analysis is more accurate at large expansions.

In Figure 4 we compare the results of SB2013 (their Figure 4) to the equation

$$\Delta R_{\text{dep}} = \Delta R_0 \left[\left(1 + \eta \frac{L_{\text{dep}} \tau_{\text{dep}}}{L_{\text{eq}}} \right)^\delta - 1 \right], \quad (32)$$

with $\Delta R_{\text{dep}} \equiv \Delta R - \Delta R_0$ denoting the expansion relative to the radius without extra heat deposition ($1.25 R_J$ in our case), $\Delta R_0 = 0.30 R_J$, η an order unity fitting parameter, and $\delta = \beta(1 - \beta)/(4 - \beta b) \approx 0.15$ from Equation (31). The fraction of incident flux $L_{\text{dep}}/L_{\text{eq}}$ is given by SB2013, and the translation of deposition pressure to optical depth is done approximately by $P/g \approx \tau/\kappa$, with κ taken from Arras & Bildsten (2006), and uncertainties going into the fitting parameter η . The parameters in Figure 4, $\eta = \delta = 0.2$, are not, strictly speaking, a best fit, but only an illustration. A second fit, with $\eta = 0.25$ and the predicted $\delta = 0.15$, is also provided. This fit, however, incorporates the more accurate nonlinear radius correction (Burrows et al. 1997) to Equation (32).

While our model is not exact, as seen in Figure 4, it does manage to describe the main trends of atmospheric heating, and, given the general uncertainties and approximations of the model, it fits the numerical calculations reasonably well over several orders of magnitude in pressure level and flux. When the realistic radius-temperature relation is used, the analytically predicted power $\delta = 0.15$ fits the results adequately. With the approximated linear radius-temperature relation, however, we fit $\delta = 0.2$ to the numerical results.

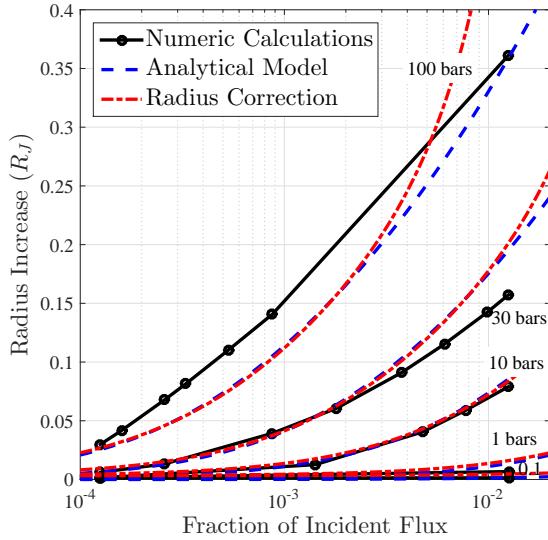


FIG. 4.— Comparison of our prediction for planet inflation (relative to $1.25 R_J$), due to heating (expressed as a fraction of the incident flux) at different pressure levels, with Spiegel & Burrows (2013), for constant surface gravity $g = 10^3 \text{ cm s}^{-2}$, effective temperature $T_{\text{eff}} = 180 \text{ K}$, and incident irradiation of HD 209458b. Our analytical model (dashed blue lines) is given by Equation (32), with fitted parameters $\eta = \delta = 0.2$. A second model (dot-dashed red lines), which takes into account the nonlinear radius-temperature relation, is also provided, with a fitted $\eta = 0.25$, and the analytically derived $\delta = 0.15$. The results of SB2013 (solid black lines, marked with circles) are taken from their Figure 4.

In the “weak heating” regime $L_{\text{dep}} \tau_{\text{dep}}/L_{\text{eq}} < 1$, it is

possible to linearize Equation (32)

$$\Delta R_{\text{dep}} \approx \delta \eta \Delta R_0 \frac{L_{\text{dep}} \tau_{\text{dep}}}{L_{\text{eq}}} = \zeta \Delta R_0 \frac{L_{\text{dep}} \tau_{\text{dep}}}{L_{\text{eq}}}, \quad (33)$$

which has the advantage of a single fitting parameter $\zeta \equiv \delta \eta \approx 0.04$, allowing for a more intuitive interpretation of the results.

6. CONCLUSIONS

In this work we presented a simplified analytical model for irradiated giant gas planets, which includes an additional heat source, deposited at an arbitrary depth inside the planet’s atmosphere.

For an irradiated planet with no extra heat sources, we found useful approximate scaling relations for the internal luminosity L_{int} of the planet, and for the radiative-convective boundary, marked by an optical depth τ_{rad} . Explicitly, the radiative-convective boundary and the internal luminosity are given by

$$\frac{L_{\text{eq}}}{L_{\text{int}}} \sim \tau_{\text{rad}} \sim \tau_c \left(\frac{U_{\text{eq}}}{U_c} \right)^{1/\beta}, \quad (34)$$

with L_{eq} , $U_{\text{eq}} \propto T_{\text{eq}}^4$ denoting the equilibrium luminosity and radiation energy density imposed by the stellar irradiation, respectively (T_{eq} is the equilibrium temperature). U_c is the central radiation energy density of the planet, and τ_c represents its optical depth (with opacities extrapolated from the outer layers of the planet inward). The power $\beta \approx 0.35$ is related to the adiabatic index of the planet and to the opacity near the planet’s edge. In addition, we identified the condition $\tau_{\text{rad}} \sim 1$, as the boundary separating insolated (irradiated) planets ($\tau_{\text{rad}} > 1$) from isolated ones ($\tau_{\text{rad}} < 1$). These relations serve as an intuitive interpretation of well-known results (Guillot et al. 1996; Burrows et al. 2000; Arras & Bildsten 2006; Fortney & Nettelmann 2010; Youdin & Mitchell 2010; Spiegel & Burrows 2013).

We addressed the effects of possible additional heat sources, parametrized by additional luminosity L_{dep} , deposited at an optical depth τ_{dep} . Such heat sources lower the internal luminosity of the planet, slow its evolutionary cooling, and are therefore candidates for solving the puzzle of over-inflated hot Jupiters (see Baraffe et al. 2010; Fortney & Nettelmann 2010; Spiegel & Burrows 2013; Baraffe et al. 2014, and references within). According to our model, the figure of merit in this context is $L_{\text{dep}} \tau_{\text{dep}}/L_{\text{eq}}$, with $L_{\text{dep}} \tau_{\text{dep}}/L_{\text{eq}} \gtrsim 1$ necessary for a significant effect. Concretely, an outer convective layer is formed in this case, between optical depths $L_{\text{eq}}/L_{\text{dep}}$ and τ_{dep} , which is equivalent to an enhanced stellar irradiation

$$\frac{L_{\text{eq}}^{\text{eff}}}{L_{\text{eq}}} = \left(\frac{T_{\text{eq}}^{\text{eff}}}{T_{\text{eq}}} \right)^4 \sim \left(1 + \frac{L_{\text{dep}} \tau_{\text{dep}}}{L_{\text{eq}}} \right)^\beta. \quad (35)$$

The internal luminosity is therefore reduced from a value of L_{int}^0 without extra heating to, roughly,

$$\frac{L_{\text{int}}}{L_{\text{int}}^0} \sim \left(1 + \frac{L_{\text{dep}} \tau_{\text{dep}}}{L_{\text{eq}}} \right)^{-(1-\beta)}, \quad (36)$$

with a further threshold of L_{int}^0 required for a significant effect.

Since the inflation of a planet, relative to its zero-temperature radius, is proportional to its central temperature, these relations provide an intuitive explanation to the dependence of inflation on the deposition depth (Guillot & Showman 2002; Baraffe et al. 2003; Wu & Lithwick 2013), and to the large equilibrium radii, in the case of very deep heating (Guillot & Showman 2002; Burrows et al. 2007; Liu et al. 2008; Spiegel & Burrows 2013).

Quantitatively, we compared our model to the recent parameter survey of Spiegel & Burrows (2013). The model, though not exact, fits the numerical results adequately, considering its simplifying assumptions and approximations.

The scaling laws presented in this work, combined with potential observational correlations (see, e.g., Laughlin et al. 2011; Schneider et al. 2011), may be used to rule out or to favor specific energy sources, or even the entire additional heat source paradigm.

This research was partially supported by ISF, ISA and iCore grants, and a Packard Fellowship. RS would like to thank the Max Planck Institute for Extraterrestrial Physics and the Humboldt Foundation for support and worm hospitality while this research was completed. We thank Peter Goldreich for insightful discussions, and the anonymous referee for helpful comments.

REFERENCES

- Anderson, D. R., Smith, A. M. S., Lanotte, A. A., et al. 2011, *MNRAS*, 416, 2108
- Arras, P., & Bildsten, L. 2006, *ApJ*, 650, 394
- Arras, P., & Socrates, A. 2009a, arXiv:0901.0735
- Arras, P., & Socrates, A. 2009b, arXiv:0912.2318
- Arras, P., & Socrates, A. 2010, *ApJ*, 714, 1
- Baraffe, I., Chabrier, G., & Barman, T. 2010, *RPPH*, 73, 016901
- Baraffe, I., Chabrier, G., Barman, T. S., Allard, F. & Hauschildt, P. H. 2003, *A&A*, 402, 701
- Baraffe, I., Chabrier, G., Fortney, J., & Sotin, C. 2014, *Protostars and Planets VI* (Tucson: Univ. Arizona Press), 763
- Barman, T. S., Hauschildt, P. H., & Allard, F. 2001, *ApJ*, 556, 885
- Batygin, K., & Stevenson, D. J. 2010, *ApJ*, 714, 238
- Batygin, K., Stevenson, D. J., & Bodenheimer, P. H. 2011, *ApJ*, 738, 1
- Bodenheimer, P., Laughlin, G., & Lin, D. N. C. 2003, *ApJ*, 592, 555
- Bodenheimer, P., Lin, D. N. C., & Mardling, R. A. 2001, *ApJ*, 548, 466
- Budaj, J., Hubeny, I., & Burrows, A. 2012, *A&A*, 537, A115
- Burrows, A., Guillot, T., Hubbard, W. B., et al. 2000, *ApJ*, 534, L97
- Burrows, A., Hubeny, I., Budaj, J., & Hubbard, W. B. 2007, *ApJ*, 661, 502
- Burrows, A., Marley, M., Hubbard, W. B., et al. 1997, *ApJ*, 491, 756
- Chabrier, G., & Baraffe, I. 2007, *ApJ*, 661, L81
- Chabrier, G., Barman, T., Baraffe, I., Allard, F., & Hauschildt, P. H. 2004, *ApJ*, 603, L53
- Chan, T., Ingemys, M., Winn, J. N., et al. 2011, *ApJ*, 141, 179
- Chandrasekhar, S. 1939, *An Introduction to the Study of Stellar Structure* (Chicago, IL: Univ. Chicago Press)
- Crossfield, I. J. M., Knutson, H., Fortney, J., et al. 2012, *ApJ*, 752, 81
- Dobbs-Dixon, I., Agol, E., & Burrows A. 2012, *ApJ*, 751, 87
- Fortney, J. J., & Nettelmann, N. 2010, *Space Sci. Rev.*, 152, 423
- Gu, P., Lin, D. N. C., & Bodenheimer, P. H. 2003, *ApJ*, 588, 509
- Guillot, T. 2005, *AREPS*, 33, 493
- Guillot, T. 2010, *A&A*, 520, A27
- Guillot, T., Burrows, A., Hubbard, W. B., Lunine, J. I., & Saumon, D. 1996, *ApJ*, 459, L35
- Guillot, T., Gautier, D., Chabrier, G., & Mosser, B. 1994, *Icarus*, 112, 337
- Guillot, T., & Havel, M. 2011, *A&A*, 527, A20
- Guillot, T., & Showman, A. P. 2002, *A&A*, 385, 156
- Hanel, R. A., Conrath, B. J., Herath, L. W., Kunde, V. G., & Pirraglia, J. A. 1981, *J. Geophys. Res.*, 86, 8705
- Hansen, B. M. S. 2008, *ApJS*, 179, 484
- Hartman, J. D., Bakos, G. À., Torres, G., et al. 2011, *ApJ*, 742, 59
- Huang, X., & Cumming, A. 2012, *ApJ*, 757, 46
- Hubbard, W. B. 1968, *ApJ*, 152, 745
- Hubbard, W. B. 1977, *Icarus*, 30, 305
- Hubeny, I., Burrows, A., & Sudarsky, D. 2003, *ApJ*, 594, 1011
- Ibgui, L., & Burrows, A. 2009, *ApJ*, 700, 1921
- Ibgui, L., Burrows, A., & Spiegel, D. M. 2010, *ApJ*, 713, 751
- Ibgui, L., Spiegel, D. M., & Burrows, A. 2011, *ApJ*, 727, 75
- Jackson, B., Greenberg, R., & Barnes, R. 2008, *ApJ*, 681, 1631
- Kippenhahn, A., & Weigert, A. 1994, *Stellar Structure and Evolution* (Berlin: Springer)
- Laughlin, G., Crismani, M., & Adams, F. C. 2011, *ApJ*, 729, L7
- Laughlin, G., Wolf, A., Vanmunster, T., et al. 2005, *ApJ*, 621, 1072
- Leconte, J., & Chabrier, G. 2012, *A&A*, 540, A20
- Leconte, J., Chabrier, G., Baraffe, I., & Levard, B. 2010, *A&A*, 516, A64
- Liu, X., Burrows, A., & Ibgui, L. 2008, *ApJ*, 687, 1191
- Marleau, G. D., & Cumming, A. 2014, *MNRAS*, 437, 1378
- Matzner, C. D., & McKee, C. F. 1999, *ApJ*, 510, 379
- Mayne, N. J., Baraffe, I., Acreman, D. M., et al. 2014, *A&A*, 561, A1
- Mayor, M., & Queloz, D. 1995, *Nature*, 378, 355
- Miller, N., Fortney, J. J., & Jackson, B. 2009, *ApJ*, 702, 1413
- Padmanabhan, T. 2000, *Theoretical Astrophysics, Volume 1: Astrophysical Processes* (Cambridge: Cambridge Univ. Press)
- Padmanabhan, T. 2001, *Theoretical Astrophysics, Volume 2: Stars and Stellar Systems* (Cambridge: Cambridge Univ. Press)
- Peebles, P. J. E. 1964, *ApJ*, 140, 328
- Perez-Becker, D., & Showman, A. P. 2013, *ApJ*, 776, 134
- Perna, R., Heng, K., & Pont, F. 2012, *ApJ*, 751, 59
- Perna, R., Menou, K., & Rauscher, E. 2010, *ApJ*, 719, 1421
- Rauscher, E., & Menou, K. 2013, *ApJ*, 764, 103
- Rauscher, E., & Showman, A. P. 2014, *ApJ*, 784, 160
- Rogers, T. M., & Showman, A. P. 2014, *ApJ*, 782, L4
- Saumon, D., Hubbard, W. B., Burrows A., et al. 1996, *ApJ*, 460, 993
- Schneider, J., Dedieu, C., Le Sidaner, P., Savalle, R., & Zolotukhin, I. 2011, *A&A*, 532, A79
- Showman, A. P., & Guillot, T. 2002, *A&A*, 385, 166
- Socrates, A. 2013, arXiv:1304.4121
- Spiegel, D. S., & Burrows, A. 2010, *ApJ*, 722, 871
- Spiegel, D. S., & Burrows, A. 2012, *ApJ*, 745, 174
- Spiegel, D. S., & Burrows, A. 2013, *ApJ*, 772, 76
- Stevenson, D. J., & Salpeter, E. E. 1977, *ApJS*, 35, 221
- Trafton, L. M. 1964, *ApJ*, 140, 1340
- Trafton, L. M. 1967, *ApJ*, 147, 765
- Winn, J. N., & Holman, M. J. 2005, *ApJ*, 159, L159
- Wu, Y., & Lithwick, Y. 2013, *ApJ*, 763, 13
- Yoodin, A. N., & Mitchell, J. L. 2010, *ApJ*, 721, 1113